

## Adaptive-Optics Compensation through a High-Gain Raman Amplifier

The applicability of Raman amplification to the problem of high-power laser propagation through a turbulent atmosphere was investigated in a two-part experimental program. The goal of the program was to determine the extent of phasefront preservation possible in a high-gain Raman amplifier. The utility of an unconventional approach to adaptive-optics compensation, known as "Raman look-through," was examined. The Raman look-through technique, which combines conventional adaptive optics using a deformable mirror and wavefront sensor with the nonlinear process of stimulated Raman scattering, performs a wavefront correction on the low-power input to a Raman amplifier, and then amplifies the corrected beam.

The first part of the experimental program determined the degree of phasefront preservation in a high-gain Raman amplifier. The phasefront of the input beam to a Raman amplifier was deliberately aberrated, and the phasefront of the amplified output beam was measured and compared to the input beam. The comparisons indicate that, under the proper conditions, a high degree of phasefront preservation can be achieved.

The second part of the experimental program studied adaptive-optics compensation through a Raman amplifier. Atmospheric turbulence was simulated by specially fabricated quartz plates that produced turbulence-like phasefront distortion on a transmitted beacon. The beacon phasefront was measured by a 69-channel wavefront sensor that commanded a deformable mirror to impose the conjugate phasefront on the Stokes seed to a high-gain large-Fresnel-number Raman amplifier. After amplification, the output Stokes beam retraced the path of the beacon through the simulated turbulence. Measurements of the Stokes beam quality indicated a dramatic improvement with near-diffraction-limited performance. The results of both experiments are in good agreement with theory.

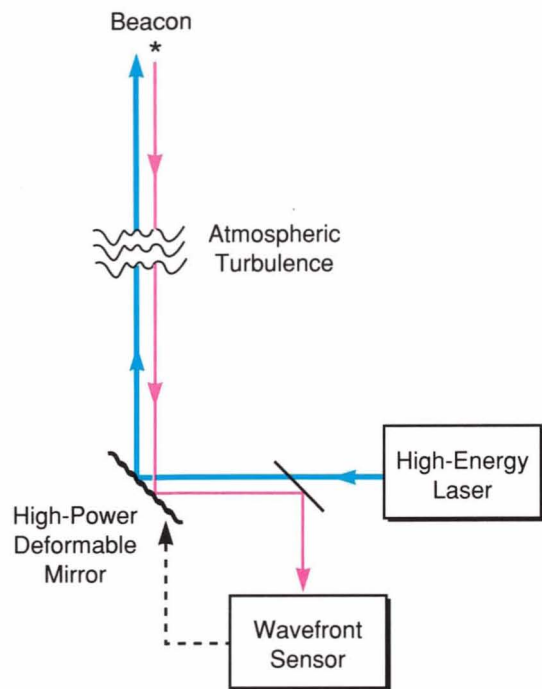
When a laser beam propagates through atmospheric turbulence, refractive-index variations along the path induce phasefront distortions that severely limit the beam quality, and therefore the focal-plane intensity, of the transmitted beam. To overcome the effects of turbulence, adaptive-optics compensation is used to correct the induced phasefront distortions and restore beam quality.

Figure 1(a) shows the traditional approach to adaptive-optics compensation [1, 2]. A wavefront sensor measures the phasefront of a beacon that has traversed the path of the outgoing laser beam. Depending on the application the beacon might be a laser mounted on a satellite,

or a star whose line of sight falls along the propagation path. The output of the wavefront sensor controls the surface of a deformable mirror that compensates for atmospheric distortions sampled by the beacon. If the outgoing laser beam is reflected by the deformable mirror before retracing the beacon path, it will be phase-compensated for the optical errors along that path, and leave the atmosphere as a nearly diffraction-limited beam.

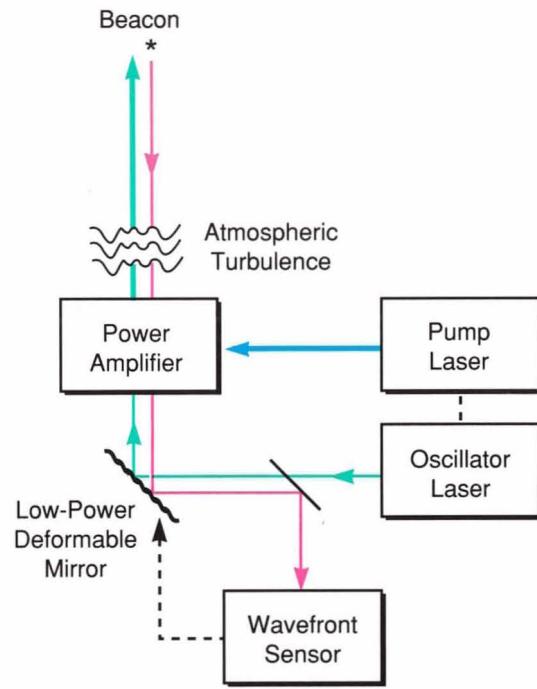
As the energy in the outgoing beam increases, two limitations to the traditional approach become increasingly significant. First, the deformable mirror must withstand the high energy and high peak power in the outgoing beam. Adap-

CONVENTIONAL APPROACH



(a)

"LOOK-THROUGH" APPROACH



(b)

Fig. 1 — (a) The traditional approach to atmospheric compensation. The deformable mirror must reflect the full output of the high-energy laser, which creates severe cooling requirements on the mirror. (b) Atmospheric compensation using an oscillator-amplifier. The deformable mirror reflects only the low-power oscillator output, which reduces the cooling requirements on the mirror.

tive control over sufficiently high-energy lasers requires that the surface of the deformable mirror be cooled. As the energy in the outgoing beam increases, so does the cooling requirement on the mirror.

A second limitation to the traditional approach is the potentially poor beam quality of the high-energy laser itself. Often in the design of large laser systems, beam-quality considerations must be compromised in favor of high energy. Because the adaptive-optics system can compensate only those distortions in the path of the beacon beam, phasefront distortions arising within the laser cavity itself are not compensated. Traditional adaptive-optics control over lasers of poor beam quality is therefore limited.

To reduce the cooling requirements on the deformable mirror, and simultaneously achieve control over a laser of poor beam quality, the adaptive-optics system can incorporate an os-

cillator-amplifier. Figure 1(b) illustrates this unconventional approach to adaptive-optics compensation. As before, a wavefront sensor measures the phasefront on the beacon (red line) and commands a deformable mirror to compensate for distortions along the propagation path. But, rather than reflect the entire high-energy beam, the deformable mirror reflects only the low-power output of the oscillator. A power amplifier then amplifies the phase-compensated oscillator output. Since the deformable mirror now controls only the low-power beam, and not the entire output beam, cooling requirements on the mirror are reduced. In addition, the oscillator output can be spatially filtered before adaptive compensation, which avoids the beam-quality limitations of the high-energy laser itself.

The approach to the oscillator-amplifier configuration used in these experiments utilizes

stimulated Raman scattering (SRS) in what is called "Raman look-through." SRS is a nonlinear optical scattering process that couples two beams traversing a Raman-active medium that serves as an amplifier. The nonlinear response of the medium amplifies one beam (the oscillator) at the expense of the other (the pump). See the adjoining box for an explanation of stimulated Raman scattering.

To be useful in adaptive-optics compensation, the Raman look-through technique must satisfy two basic requirements. First, the amplifier must efficiently transfer energy from the pump laser to the oscillator input. Since only the oscillator beam is phase-compensated by the deformable mirror, unconverted pump radiation is lost from the system. The actual energy-conversion requirement depends on the particular application, but, in general, 50% or more energy conversion is considered efficient.

Second, the phasefront of the oscillator input beam must not be significantly distorted by the amplification process. The amplification must

be high fidelity even when the phasefront of the input beam has been modified by the deformable mirror. The phase and intensity distortions on the pump laser can also induce phasefront distortions on the input beam during the amplification process. Because these phasefront errors cannot be corrected by the adaptive-optics system, the quality of the atmospheric compensation is reduced.

The objective of the experiments described in this article was to determine the degree of phasefront preservation possible in a high-gain, large-Fresnel-number Raman amplifier using a pump laser of poor beam quality. The primary goal was to measure the structure and magnitude of any phasefront distortion on the amplified Stokes, and properly identify the source of the distortions. To achieve this goal we assembled experimental diagnostic hardware to measure the phase and intensity of both input and pump beams at the entrance and exit of the Raman amplifier. Measurements were made for a wide range of input phasefronts in the pres-

## Raman Scattering and Stimulated Raman Scattering

The classical Raman effect arises from inelastic scattering between a molecule and a photon of light. The molecule is left in a more highly excited state and the frequency of the scattered light is shifted to a longer wavelength, or lower energy. Because of energy conservation, the excess energy gained by the molecule exactly matches the energy lost by the scattered light. Unlike resonant excitation and fluorescence, however, energy transfer can occur for any frequency of incoming light, not just frequencies that match the molecular energy-level spacing. In 1930, C.V. Raman received the Nobel prize for his work on scattering and the discovery of

the effect that bears his name.

Stimulated Raman scattering (SRS) was discovered in 1962 by E.J. Woodbury and W.K. Ng [1]. While studying the optical Kerr effect in nitrobenzene, they observed a new frequency component in the scattered laser light. The new frequency component coincided with the Raman mode of nitrobenzene and was later identified as stimulated Raman emission [2].

Most theoretical descriptions treat SRS as a quantum-mechanical two-photon process, but it can be viewed classically as a parametric process in which two electromagnetic waves are coupled by the polarizability of

the medium. Historically, the frequency-shifted light has been called Stokes radiation if the shift is toward longer wavelengths, and anti-Stokes radiation if shifted to shorter wavelengths. This nomenclature is carried over from G. Stokes' early work in the spectroscopy of fluorescence.

### References

1. E.J. Woodbury and W.K. Ng, "Ruby Laser Operation in the Near IR," *IEEE Proc.* **50**, 2367 (1962).
2. R.W. Hellwarth, "Theory of Stimulated Raman Scattering," *Phys. Rev.* **130**, 1850 (1963).

ence of a severely distorted pump beam.

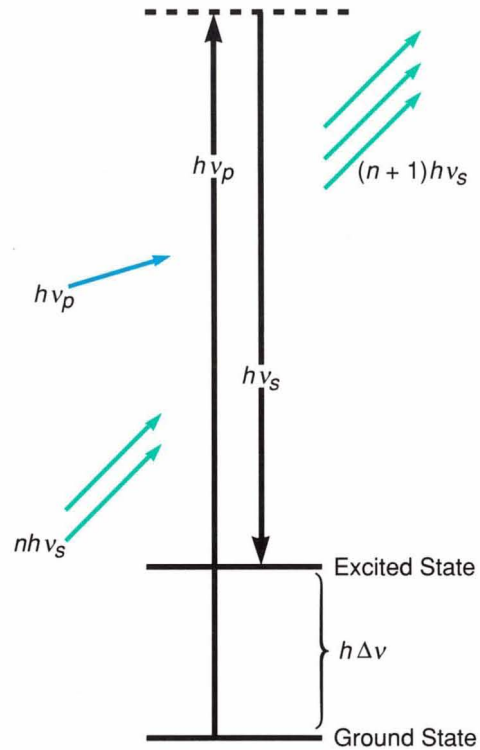
The results described in this article support the feasibility of the Raman look-through technique. The initial experiment, conducted at Lincoln Laboratory, joined the Atmospheric Compensation Experiment (ACE) adaptive-optics system with a Raman amplifier pumped by a laboratory excimer laser [3]. The second experiment, a joint effort between Lincoln Laboratory and Avco Research Laboratory, used the large xenon-fluoride excimer laser known as Scale-up to determine the amplification fidelity in a high-gain, large-Fresnel-number Raman amplifier. The Raman amplifier was then used with the ACE adaptive-optics system to investigate the utility of the Raman look-through technique. In all the experiments, a krypton-ion laser operating at 413 nm was the beacon source, and phase screens — ion-milled quartz flats — simulated the effects of atmospheric turbulence.

## Applications of Raman Amplification

### Amplification Using Stimulated Raman Scattering

Figure 2 illustrates the concept of SRS [4]. In the ordinary Raman effect a photon at the pump-laser frequency,  $\nu_p$ , scatters from an initially unexcited molecule as indicated by the solid arrow labelled  $h\nu_p$ . The molecule undergoes a transition to a more highly excited state via an intermediate transition to a virtual state. Energy is left behind in the molecule and the scattered photon is at reduced energy,  $h\nu_s$ , where  $h\nu_p = h\Delta\nu + h\nu_s$ . The scattered light is said to be at the Stokes frequency. When the intensity of the Stokes wave grows sufficiently large, the scattering process becomes stimulated and the Stokes wave, now efficiently coupled to the pump wave by the polarizability of the medium, can experience exponential gain.

In practice, SRS uses a cell of a suitable liquid or pressurized gas as the Raman medium. High-pressure hydrogen is favored for this application because of its large Raman shift —  $4,155 \text{ cm}^{-1}$  for the Q(1) vibrational transition — and its high gain coefficient —  $6 \times 10^{-3} \text{ cm/MW}$  at 400 nm. In



Where:  $\nu_p$  = Pump Frequency  
 $\nu_s$  = Stokes Frequency

Fig. 2 — An illustration of the concept of stimulated Raman scattering.

the experiments described in this article the Raman medium was always hydrogen.

Figure 3 illustrates the typical approach to Raman amplification. A low-power sample of the laser is separated from the main output beam, either by a partial reflector or, more commonly, by picking off a small subaperture of the full beam. The low-power sample passes through a cell containing the Raman-active medium, with conditions adjusted so that the gain  $G$ , where gain is the product of gain coefficient, beam intensity, and path length ( $G = gIL$ ), exceeds a threshold value.

With properly chosen geometry, a sizable fraction (>30%) of the input beam to the Raman medium can be shifted to the Stokes frequency  $\nu_s$ . The Stokes beam thus obtained is then recombined with the remainder of the pump beam in a second Raman cell, referred to as the

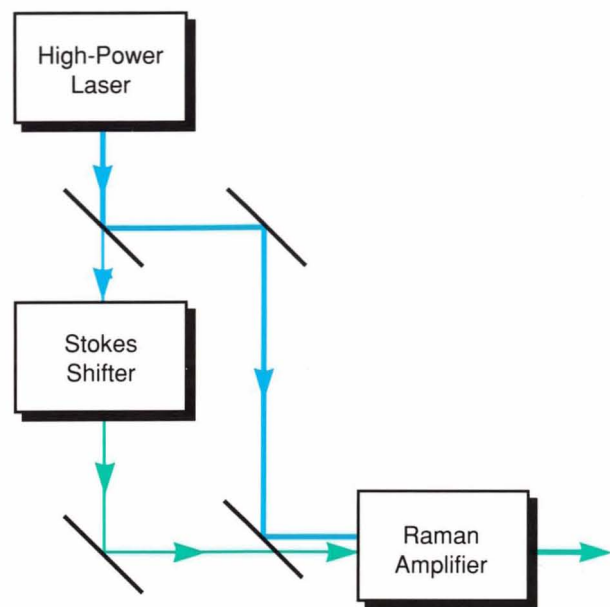


Fig. 3 — The usual laboratory configuration for Raman amplification. A low-power sample of the high-power beam is diverted through a Stokes shifter. The output Stokes beam is recombined with the remainder of the high-power laser in a Raman amplifier.

Raman amplifier. The injected Stokes beam serves as a seed, that, under proper conditions, can be efficiently amplified so that more than 80% of the input pump energy is converted to Stokes light [5]. In this way, Raman amplification is used to shift a laser's output frequency to a value more suited to the particular application [6].

### Raman Beam Cleanup

The poor quality of a laser beam wavefront can be improved by a technique called Raman beam cleanup [7], shown in Fig. 4(a). As before, a low-power sample of the laser is used to pump a Stokes cell, but now the Stokes-shifted output is spatially filtered and precisely collimated before being recombined with the remainder of the pump beam in the amplifier. The goal is to amplify the diffraction-limited Stokes seed without distorting its phasefront. Successful application of Raman beam cleanup can improve the intensity of the laser beam by several orders of magnitude.

The focal-plane intensity  $I$  is proportional to beam energy  $E$  divided by the focal-spot area,  $(\lambda\beta)^2$ , where  $\lambda$  is the wavelength and  $\beta$  is the beam quality. The conversion efficiency  $\eta$  is defined as the ratio of output Stokes energy to input laser energy,

$$\eta = \varepsilon \cdot \frac{E_s}{E_p}$$

where the quantum efficiency  $\varepsilon$  is the ratio of pump wavelength to Stokes wavelength,  $\lambda_p/\lambda_s$ . The amplification fidelity  $F$  is the ratio of the input and output focal-spot areas,  $\beta_{si}^2/\beta_{so}^2$ . Thus, an amplification fidelity of unity implies no degradation in the phasefront of the amplified Stokes beam. The intensity of the amplified Stokes beam is then given by

$$I_s = \frac{E_s}{(\lambda_s \beta_{so})^2} = \frac{\eta E_p F}{(\lambda_s \lambda_p \beta_{si}^2)}$$

The focal-plane intensity increase for an initially diffraction-limited seed, where  $\beta_{si}^2 = 1$ , is then given by

$$\frac{I_s}{I_p} = \varepsilon \eta F \beta_p^2$$

For a XeCl excimer-pumped hydrogen amplifier with a pump-laser beam quality  $\beta_p^2$  of 50, a conversion efficiency  $\eta$  of 0.5, and amplifier fidelity of 0.8 units, the intensity is increased by a factor of 18. The break-even point for this process is given by  $\eta F > 1/\varepsilon\beta_p^2$ . Thus, for a badly aberrated laser ( $\beta_p^2$  large), the product of conversion efficiency and amplification fidelity need not be very large in order to achieve an overall improvement in intensity.

### Raman Look-Through

The technique of Raman beam cleanup relies on the initially unaberrated phasefront of the Stokes beam remaining undistorted by the amplification process. A more complicated Stokes phasefront, such as that produced by atmospheric turbulence, can also be amplified without distortion. In the Raman look-through approach to atmospheric compensation, the adaptive-optics phase sensor "looks through"

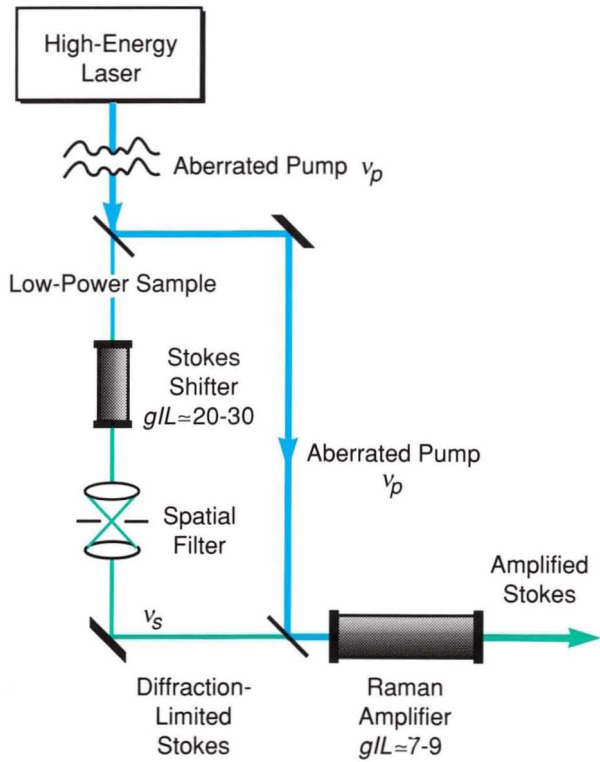


Fig. 4 — (a) An illustration of the technique of Raman beam cleanup. The output of the Stokes shifter is spatially filtered before amplification.

the Raman amplifier to monitor the atmospheric turbulence. Figure 4(b) shows the concept of Raman look-through. The wavefront sensor receives a beacon (red line) whose phasefront has been distorted by passage through turbulence. The phase sensor adjusts the surface of the deformable mirror to compensate for the aberrations on the beacon wavefront. The diffraction-limited Stokes seed then reflects from the surface of the deformable mirror and receives the appropriate phasefront for turbulence compensation. The precompensated Stokes seed is then amplified and passed back through the turbulence. For this approach to be successful, both the adaptive-optics compensation and the degree of Stokes-phasefront preservation during high-gain amplification must be high in quality.

The performance of an adaptive-optics system is determined by spatial resolution, temporal bandwidth, and spatial overlap between return

beacon and outgoing beam. Phasefront preservation, however, is determined almost entirely by the geometry of the amplifier. In a collimated geometry the most basic requirement for the amplifier is that the length of the amplifier must be well within the near field of the smallest scale structure on either the pump beam or the Stokes beam.

The constraint on amplifier geometry determines the Fresnel number of the amplifier. The Fresnel number is defined as  $F = D^2 / \lambda L$ , where  $D$  is the beam diameter,  $\lambda$  is the wavelength, and  $L$  is the Raman cell length. By using the expression for the Fresnel number  $F$  and the desired gain,  $G = gIL$ , an estimate of input laser power  $P$  can be found to be

$$P = \frac{\lambda F G}{g}$$

$P$  is the power required to achieve the desired gain,  $G$ , at the chosen Fresnel number. For a given input laser power, this expression also provides an estimate of the highest achievable gain at a particular Fresnel number.

The Raman look-through approach to atmospheric compensation has two principal advantages. First, since the deformable mirror reflects only a portion of the entire output of the laser, cooling requirements are reduced. Second, since the Stokes seed is spatially filtered before pre-compensation, there is no performance penalty due to the uncompensated aberrations of the laser itself.

### Potential Limitations

Two requirements are important in applications of Raman beam cleanup or Raman look-through: 1) efficient energy conversion from pump beam to Stokes beam, and 2) absence of induced phase distortion in the Stokes beam due to pump-phase or intensity aberrations.

### Energy-Conversion Efficiency

The threshold intensity for a Stokes oscillator (or single-pass shifter), where the Stokes wave grows from spontaneous Raman scattering or noise, is independent of the pump-laser linewidth [8]. The linewidth independence occurs

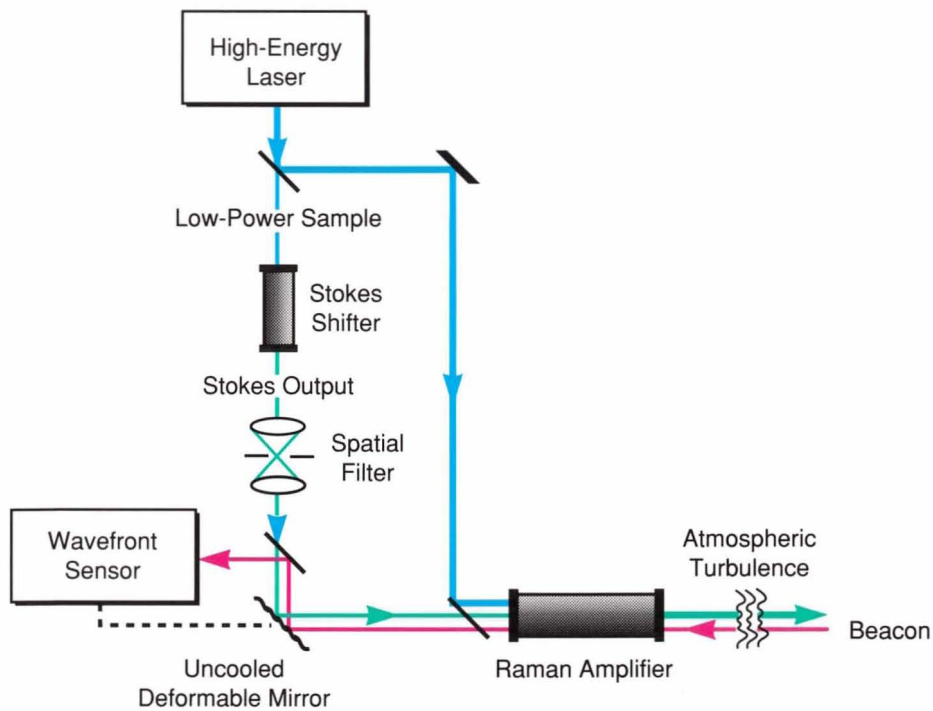


Fig. 4 — (b) The Raman look-through approach to atmospheric compensation. The adaptive-optics wavefront sensor and deformable mirror control the Stokes input to a Raman amplifier. The primary advantage to Raman look-through is that the deformable mirror reflects only the low-power Stokes beam and therefore does not require cooling.

despite the fact that only Stokes modes having optimum phase relationships with the pump are amplified. The nature of Stokes noise implies that components with the correct phase relationships are always present.

In a Raman amplifier, however, the Stokes wave is already prepared, and the initial phases may not be optimum. In cases where the Stokes phases are uncorrelated, the growth of the Stokes wave (for weak pump depletion) is given by

$$I_s(z) = I_s(0) \cdot \frac{\exp[g I_L(0) z]}{N}$$

where  $N$  is the number of longitudinal modes composing the laser linewidth.

The optimum phase relationship between the Stokes and pump modes corresponds to a Stokes temporal profile proportional to that of the pump at every point in time [9]. By precisely overlapping the temporal fine structure of the Stokes and pump pulses at the entrance to the

amplifier, monochromatic gains ( $N = 1$ ) can be achieved. The precision with which the overlap must be made is roughly equal to the coherence length of the pump. Experimentally, this precision is accomplished by carefully matching the path lengths of the pump and Stokes beams. Therefore, two major factors govern the amplifier performance and the conversion efficiency: the gain  $G$  and the accuracy of the path matching between pump beam and Stokes beam.

### Phasefront Preservation

The goal of beam cleanup is to realize efficient pump-to-Stokes energy conversion without simultaneous transfer of pump-phase or intensity aberrations. Two principal mechanisms transfer pump-phase or intensity aberrations onto the Stokes beam: spatial variation in refractive index of the Raman medium and diffraction effects.

When the molecules that compose the Raman

medium exhibit a significant difference in the refractive index of the initial and final states (as in hydrogen), a process known as transient refractivity or saturated dispersion becomes important [10]. If the pump fluence is large (approximately  $5 \text{ J/cm}^2$ ) and the molecular dephasing time is on the order of the pulse length, a significant population of molecules in the excited state can be produced. Because the buildup is greatest where the pump intensity is largest, the spatial characteristics of the Raman medium refractive-index variation will be similar to the pump-intensity profile. The spatial variation in refractive index then distorts the Stokes phasefront. If the variations in pump intensity form a smooth Gaussian profile, the resulting Stokes distortion will be primarily focus; if the pump-intensity variations are of smaller scale, the Stokes distortion will be more random in nature.

In addition to transient refractivity, the effects of diffraction within the amplifier can also distort the Stokes-beam phasefront. Because of the nature of the SRS gain, pump-intensity aberrations result in Stokes-intensity aberrations, which then diffract as the Stokes beam propagates. As a result, the phase profile is modified.

Both the transverse extent and the depth of modulation of the distortion determine the scale-size  $d$  of the pump-beam aberrations. To avoid the diffractive effects of these aberrations, the Fresnel number,  $F_d = d^2/\lambda L$  (where the Raman cell length  $L = G/gl$ ), must be kept large. Combining the expression for the Fresnel number with the pump intensity  $P_L/D^2$  (where  $P_L$  is the pulse power and  $D$  is the beam diameter) provides a rough estimate of the power required to achieve a particular gain at a specific Fresnel number

$$P_L = \left(\frac{D}{d}\right)^2 \cdot \frac{\lambda F_d G}{g} .$$

For a xenon-fluoride excimer laser of 353-nm wavelength, a hydrogen gain coefficient of 0.006 cm/MW; an overall gain of  $G = 15$ ; spatial frequency,  $D/d$ , of 8; and a Fresnel number of 10, the required power is approximately 60 MW.

## Experimental Configuration

Figure 5 shows an overview of the experimental configuration. The output of the beacon laser (red line) passes through the phase screens that simulate turbulence, and then backwards through the Raman amplifier before reflecting from the deformable mirror and entering the wavefront sensor. When the high-power excimer laser fires, a small subaperture of its output is diverted through a Stokes generator. The resulting Stokes beam (green line) reflects from the deformable mirror before being recombined with the main beam (blue line) in the Raman amplifier. At the end of the amplifier, a sample of the Stokes beam passes back through the phase screens and into the diagnostics.

### Excimer-Laser System

For these experiments it was important to investigate the Raman look-through technique with laser energies higher than allowed by the traditional approach to adaptive optics. The laser power must also satisfy the requirements of the previous section. After considering several candidate lasers, we selected one built and operated by the Avco Research Laboratory in Everett, Mass. Besides the laser itself, an important factor in this decision was the experimental background of the Avco team. A great deal of practical experience had been gained in previous Raman amplification experiments. The laser, shown in Fig. 6, is a xenon-fluoride (XeF) excimer laser that operates with a mixture of neon, xenon, and nitrogen trifluoride in an unstable resonator configuration.

Because of the high cost of large optical elements, the output of the laser was restricted to a 30-cm-diameter aperture for these experiments. Energy through the 30-cm aperture is approximately 500 J, with the majority of the energy lying in the 353-nm band. Lasing is excited by 400-kV electrons produced by a Marx-bank-driven, pulse-forming network. The electrons are produced by a cold-cathode discharge in the presence of a 2.5-kG magnetic field. Because of space-charge effects during the 1.6- $\mu\text{s}$  pulse, the temporal energy profile as-

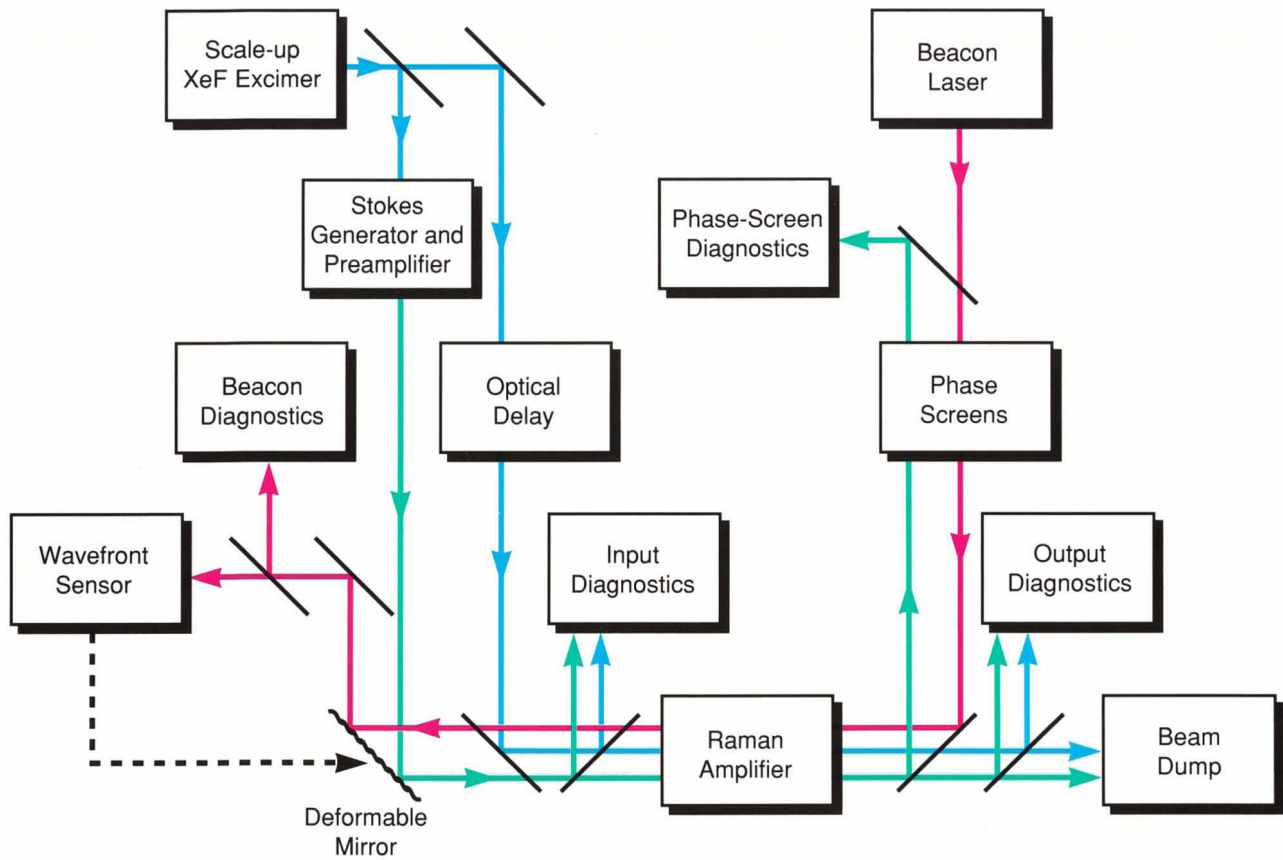


Fig. 5 — An experimental overview. The red line indicates the path of the reference beacon, the green line indicates the path of the Stokes beam, and the blue line indicates the path of the pump beam.

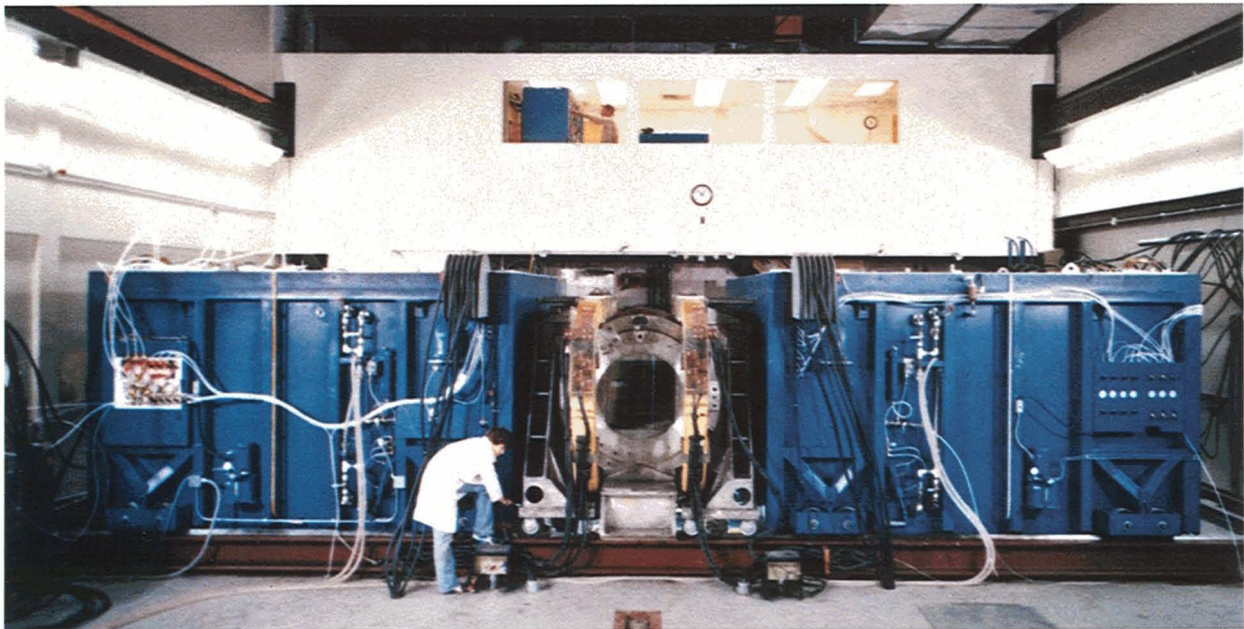


Fig. 6 — The Avco Research Laboratory xenon-fluoride excimer laser, known as Scale-up. Photo courtesy of Avco Research Laboratory.

sumes the characteristic ramp shape shown in Fig. 7(a).

### Stokes Generator and Raman Amplifier

To produce the Stokes beam, a 3-J sample of the excimer output is diverted from the main beam and passed through a Stokes shifter. The approximately 100-mJ Stokes-shifted output is recollimated, adjusted in size, and reflected from the deformable mirror. The beam serves as the seed to the Raman amplifier. The remainder of the excimer beam is also adjusted in size, polarized, and passed through an optical delay line. The 150 J that remain will serve as the pump for the Raman amplifier.

Figure 7 illustrates gain characteristics of the main Raman amplifier, with plots of the temporal energy profiles of the pump and Stokes pulses. Figure 7(a) shows the input and output (depleted) pump temporal profiles. As indicated in the figure, approximately half of the usable 150-J pump beam is converted to Stokes radiation. The difference between the input and output pump energy is equal to the output (amplified) Stokes energy. Figure 7(b) is the temporal profile of the amplified Stokes beam recorded at the amplifier exit. The integrated energy of the amplified Stokes pulse is approximately 75 J,

which shows that roughly 50% of the pump beam is converted in the amplifier.

The phase and intensity profiles of the pump and Stokes beams are measured at the entrance and exit of the Raman amplifier. Figure 8 shows a sample of the pump and Stokes data. The severely reduced beam quality of the pump is due primarily to the poor quality of the polarizers. Since one of our experimental objectives was to investigate Stokes-phasefront preservation in the presence of an aberrated pump beam, the unexpectedly poor quality of the polarizers provided a convenient means of introducing pump-beam distortion.

### Beacon Laser and Focal-Plane Diagnostics

Figure 9(a) shows a schematic of the beacon, phase screens, and focal-plane diagnostics. The beacon source is a continuous-wave krypton-ion laser operating at 413 nm. The 413-nm line was chosen because of its proximity to the Stokes line at 414 nm. The beacon laser output (red line) first passes through a polarization rotator adjusted to produce p-polarized light (horizontally polarized relative to the optical table), before being spatially filtered and expanded to a diameter of 1 cm. The beacon passes through a polarizing beam splitter, merges with

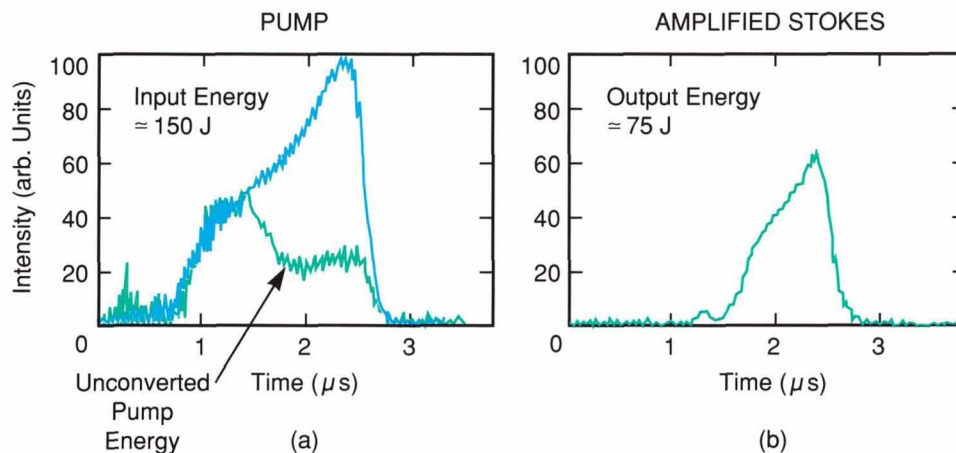


Fig. 7 — (a) Gain characteristics of the main Raman amplifier. The input and depleted output pump are shown. (b) The temporal profile of the amplified Stokes beam recorded at the amplifier exit. The conversion efficiency for the Stokes pulse is approximately 50%, so that approximately half of the input pump beam is converted to a Stokes beam.

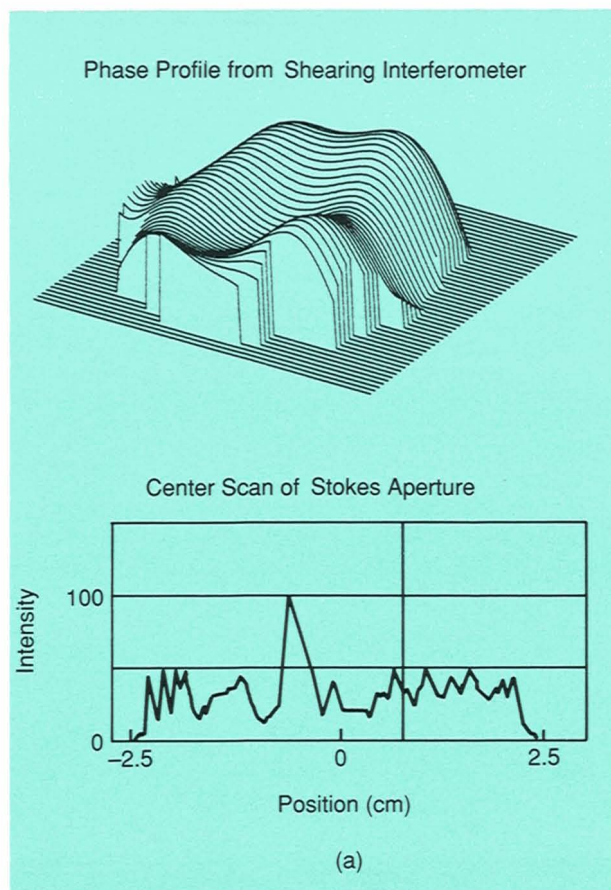


Fig. 8 — (a) The Stokes-phase and intensity profiles recorded at the entrance to the Raman amplifier. The Stokes beam contains approximately 100 mJ of polarized, 414-nm energy. The Stokes-phase profile is mildly distorted, with a 0.4-wave peak-to-peak and 0.1-wave rms error.

the incoming amplified Stokes beam (green band), and then passes through the phase screens where it samples the simulated atmospheric turbulence.

Next, the beacon is expanded to a 5-cm diameter and re-imaged into the Raman amplifier and ultimately into the wavefront sensor. The re-imaging is critical to any adaptive-optics experiment, since without it some of the high spatial-frequency phasefront information might be lost through diffraction and not received by the wavefront sensor.

When the precompensated Stokes beam is amplified during a laser pulse, a sample of the output Stokes is taken at the output of the amplifier and made to retrace the beacon path back through the phase screens. The vertically

or s-polarized Stokes beam then reflects from the polarizing beam splitter and enters the diagnostics. The diagnostics consist of solid-state arrays to record the near-field and far-field intensities, and a shearing interferometer to record the phasefront of the amplified Stokes beam. The far-field irradiance is also recorded on film. Figure 9(b) shows a photograph of the beacon and diagnostic subsystem.

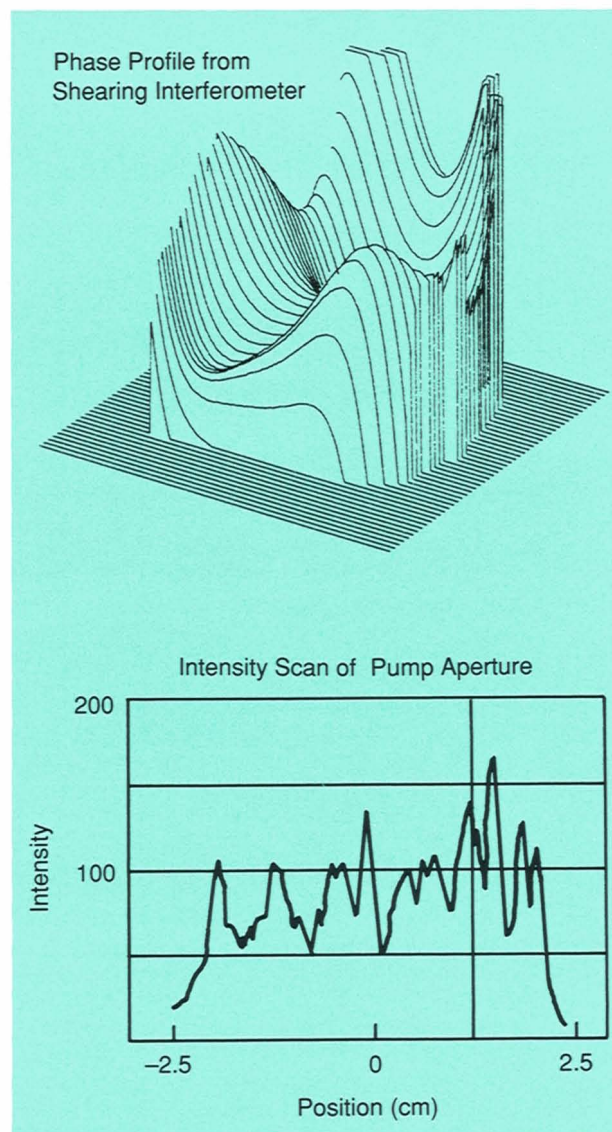


Fig. 8 — (b) The phase and intensity profiles of the pump beam. The pump beam contains approximately 150 J of polarized, 353-nm energy. The pump-phase profile is severely distorted, with a 2.0-wave peak-to-peak and 0.6-wave rms error.

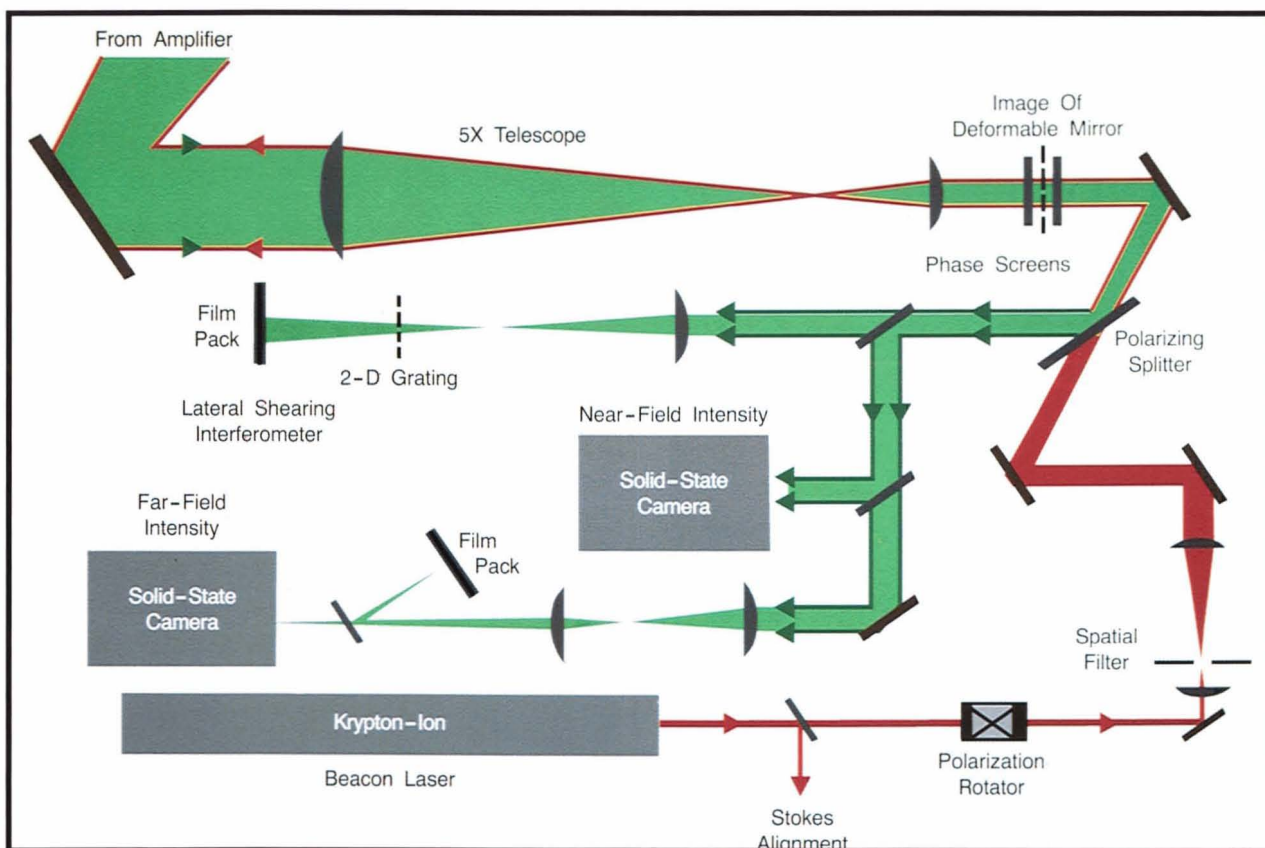


Fig. 9 — (a) Optical configuration for beacon laser and focal-plane diagnostics. The red line indicates the path of the beacon, and the green band indicates the path of the Stokes beam.

### Adaptive-Optics System

Figure 10(a) shows a schematic diagram of the adaptive-optics subsystem, while Fig. 10(b) is a photograph of the experimental setup. The beacon (red line), after passing backward through the Raman amplifier, follows the path of the Stokes beam through the pump/Stokes dichroic, and is de-expanded by the Stokes telescope before passing through an additional set of relay optics. The purpose of the relay optics is to make the phase screens, amplifier exit, and deformable mirror all conjugate image planes. After reflection from the deformable mirror, the (p-polarized) beacon travels through a polarizing beam splitter and enters the wavefront sensor. A beam splitter at the entrance to the wavefront sensor removes a sample of the beacon and focuses it onto a solid-state array. The beacon's far-field irradiance is recorded and used to determine the performance

of the adaptive-optics system.

The wavefront reconstructor and deformable mirror servoelectronics use the phasefront gra-

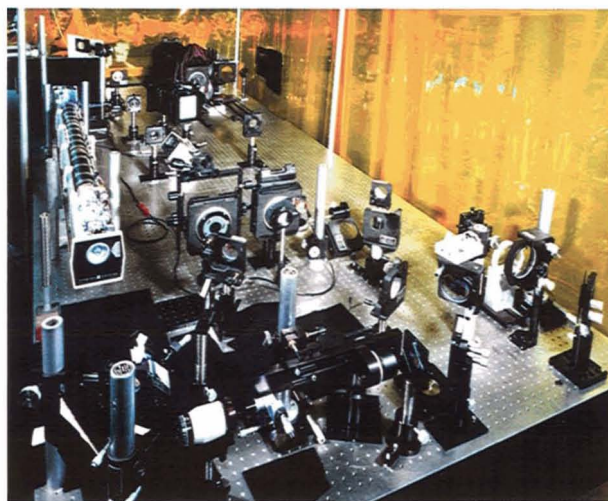


Fig. 9 — (b) Photograph of beacon and diagnostic table.

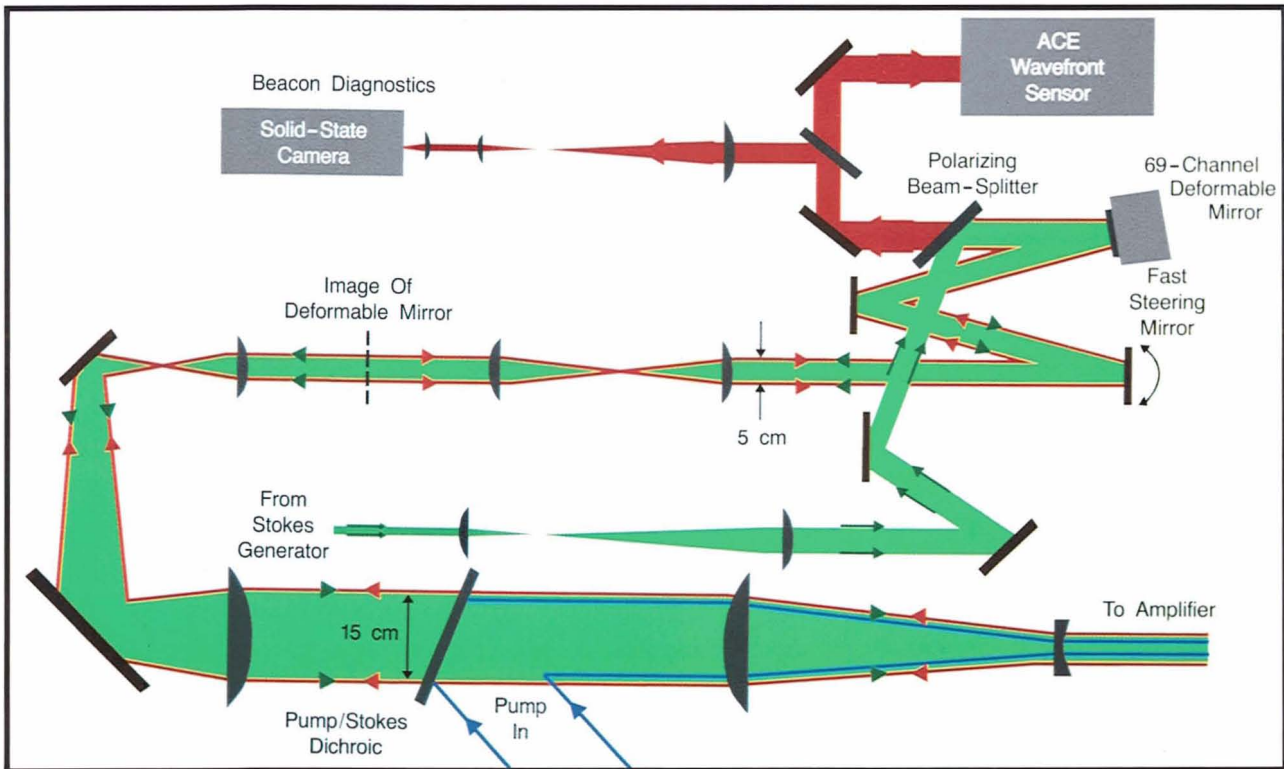


Fig. 10 — (a) Optical layout of adaptive-optics system. The red line indicates the path of the beacon, the green band indicates the path of the Stokes beam, and the blue line indicates the path of the pump beam.

dients measured by the wavefront sensor to compute and apply the appropriate voltage to each deformable-mirror actuator. The system then drives the deformable mirror to a surface figure that is the conjugate of the beacon phasefront.

When Scale-up is fired, the Stokes output from the Stokes generator (green line) enters the path of the returning beacon. The Stokes beam reflects from the deformable-mirror surface, where it acquires the appropriate phasefront to compensate for the simulated turbulence it will encounter after amplification. The preamplified, precompensated Stokes beam is then recombined with the 353-nm pump beam and the two beams are then passed through the Raman amplifier.

## Results

### Phase-Preservation Experiments

The first tests of phase preservation during the

amplification process were conducted with the unaberrated Stokes beam shown in Fig. 8. The Stokes beam and pump beam were temporally correlated and de-expanded to a 3.5-cm diame-



Fig. 10 — (b) Photograph of the adaptive-optics system.

ter before entering the main amplifier. The 3.5-cm beam diameter and a cell length of 4.44 m created a Fresnel number of 780, and resulted in a 60% conversion efficiency from pump beam to Stokes beam.

Figure 11 illustrates the results of this high-gain beam cleanup experiment. The far-field-intensity profiles in Fig. 11(a) and (b) are deduced from the near-field phase measurements at the entrance and exit of the main amplifier. The data show that a near-diffraction-limited input Stokes seed ( $\approx 1.5$  times the diffraction limit) was amplified by a very aberrated pump beam ( $\approx 0.6$  wave rms), with the resulting amplified Stokes beam emerging also as near-diffraction-limited ( $\approx 1.7$  times the diffraction limit). A slight difference between the input and amplified Stokes focal spots is detectable; detailed analyses of the measured wavefronts reveal a phase difference of less than 0.1 wave rms. For comparison, Fig. 11(c) presents a calculated far-field-intensity for the input pump beam. Clearly, significant beam cleanup occurs. Using the definitions outlined in the section on "Raman Beam Cleanup," the system focal-plane intensity has increased by a factor of approximately 200.

In subsequent measurements, an aberrator plate (a segment of glass selected for its surface figure) was deliberately inserted into the Stokes beam path to distort the Stokes phasefront.

Figure 12(a, b) shows the measured input and output Stokes phasefronts resulting from the aberration plate. Qualitatively, these beams appear quite similar. A quantitative comparison is made by subtracting one of the two phase measurements from the other.

Figure 12(c) shows the results of the phase subtraction. If the amplification process caused no distortions, the phase profile obtained by subtracting "phase in" from "phase out" would be flat across the wavefront. Any deviation from a flat wavefront represents the degree of distortion. In this case, the distortion is small with a residual phasefront error of 0.1 wave rms.

The data from the phase print-through experiment have been compared with the results of a numerical computer calculation [12]. The computer calculation incorporates three spa-

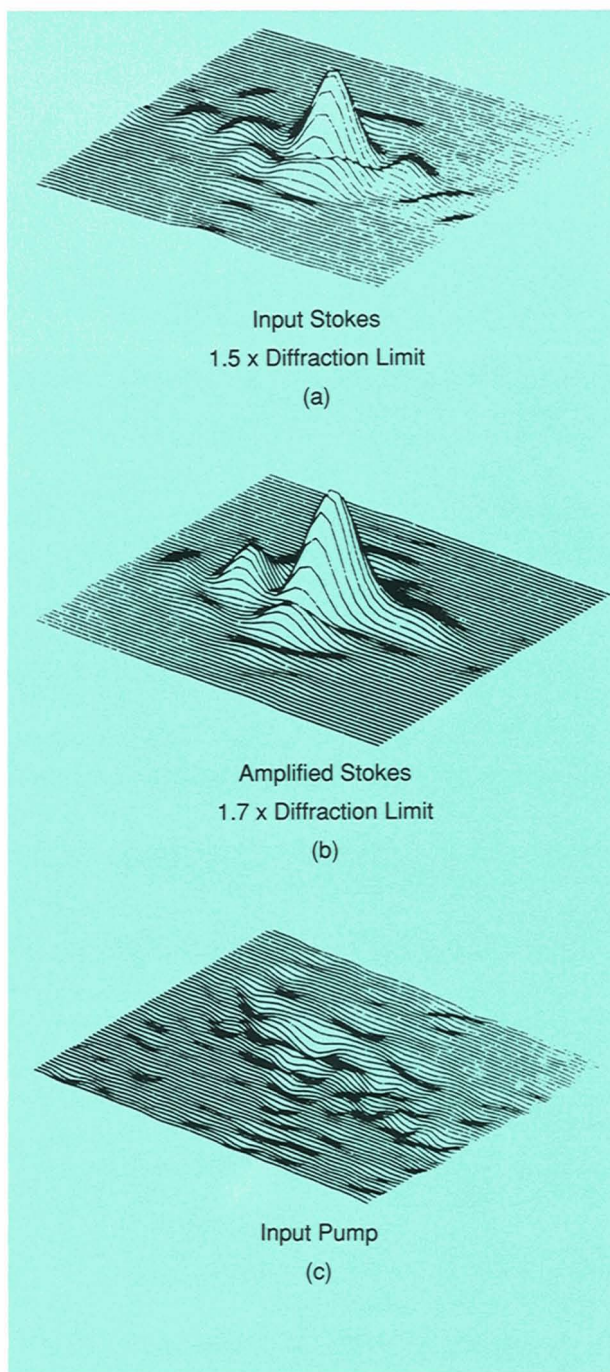


Fig. 11 — (a) Calculated far-field irradiance of input Stokes beam, based on interferometric measurement. (b) Calculated far-field irradiance of output or amplified Stokes beam, based on interferometric measurement. (c) Calculated far-field irradiance of pump beam, based on interferometric measurement.

tial dimensions and one temporal dimension in a full wave-optics treatment, including diffraction, the effects of transient refractivity,

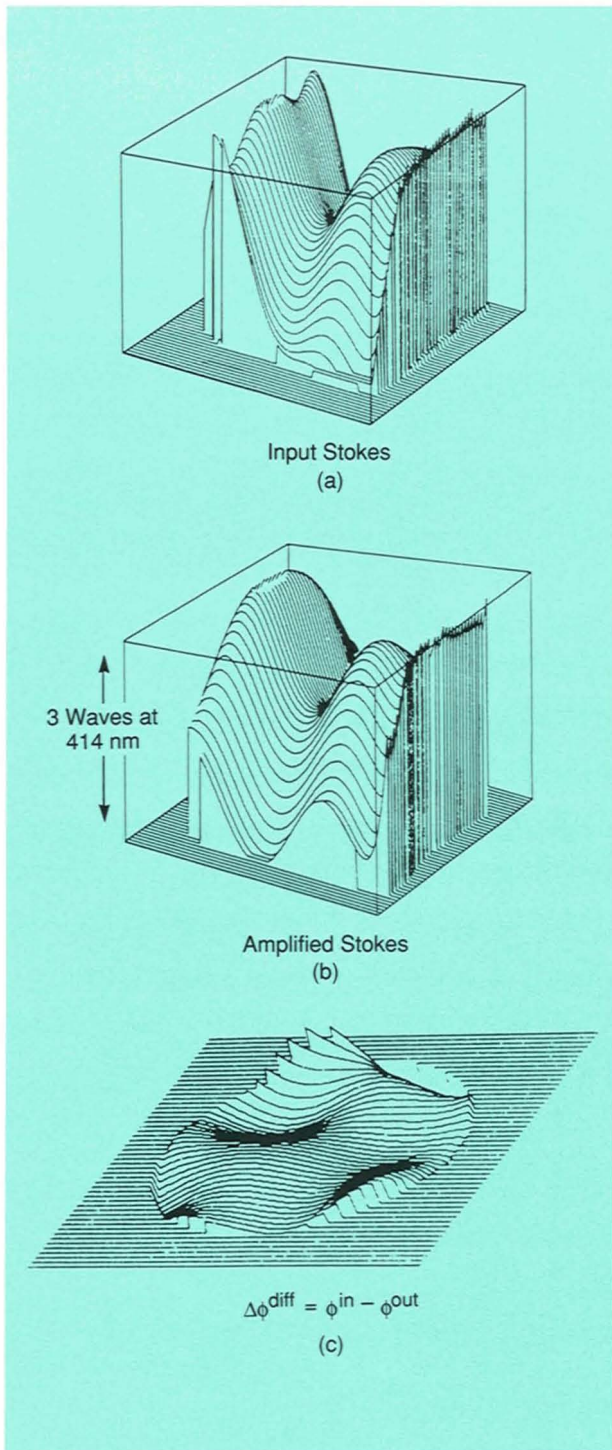


Fig. 12 — (a) Results of print-through experiment. (a) The input Stokes phasefront. (b) The amplified Stokes phasefront. (c) The difference between the input and amplified Stokes phasefronts. Over the inner 77% of the Stokes-beam aperture, the difference between the input and output Stokes wavefronts is 0.6-wave peak-to-peak and 0.1-wave rms error.

and thermal blooming.

To facilitate the comparison with experiment, the reduced experimental data were used as starting conditions for the calculation. The coefficients for a polynomial fit to the pump and Stokes phasefronts were used to generate the input phases. The pump-beam and Stokes-beam-intensity profiles used in the calculation were not reproduced exactly but were modeled by a random intensity distribution tailored to resemble closely the experimental data. The temporal profiles of the pump and Stokes beams were also modeled closely after the experiment.

Figure 13 illustrates the input and amplified Stokes wavefronts calculated in the simulation. The presence of high spatial-frequency structure on the amplified Stokes phasefront is the most noticeable effect. This structure, which is related to the intensity scintillation of the pump, is caused by the diffraction mechanism discussed in the section on applications of Raman amplification. Other simulations that use a smooth pump-intensity profile verify this conclusion. Experimentally, the low-amplitude, high spatial-frequency phase modulation is observed as a modulation in the fringe thickness of the interferogram, but it is not resolved by the wavefront reconstruction program used to reduce the data.

#### Adaptive-Compensation Experiments (Raman Look-Through)

After it was determined that an aberrated Stokes beam can be amplified without significant distortion, the adaptive-optics subsystem was used for a series of look-through experiments. As discussed above, atmospheric turbulence is simulated by passing the 413-nm beacon beam through multiple phase screens, while the screen locations are re-imaged into the Raman amplifier and onto the surface of the deformable mirror.

Figure 14 shows the performance of the adaptive-optics system. The far-field irradiance of the beacon is recorded by the solid-state array in the wavefront sensor leg (see Fig. 10), and digitized to produce the contour plots shown in Fig. 14. The upper contour plot shows the beacon focal

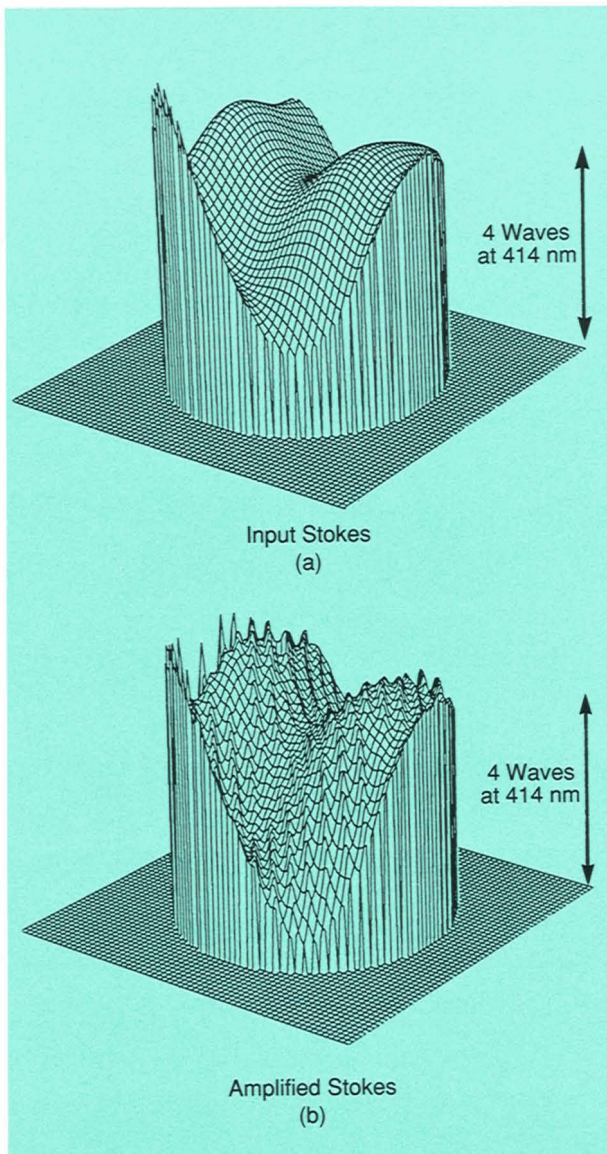


Fig. 13 — Results of computer simulations of print-through experiment. (a) Input Stokes phasefront modeled to resemble the experimental data. (b) Amplified Stokes phasefront predicted by computer simulation. The high-frequency modulation is a direct consequence of the modulated pump-beam intensity shown in Fig. 8(b).

spot without the phase-compensation loops in operation. As shown in the figure, the turbulence-like phasefront distortion suffered by the beacon as it traverses the phase screen results in a far-field irradiance roughly 17 times the diffraction-limited area. With the phase-compensation circuits activated, the spot size decreases dramatically. As indicated by the vertical arrow, the focal-spot area of the beacon decreases to

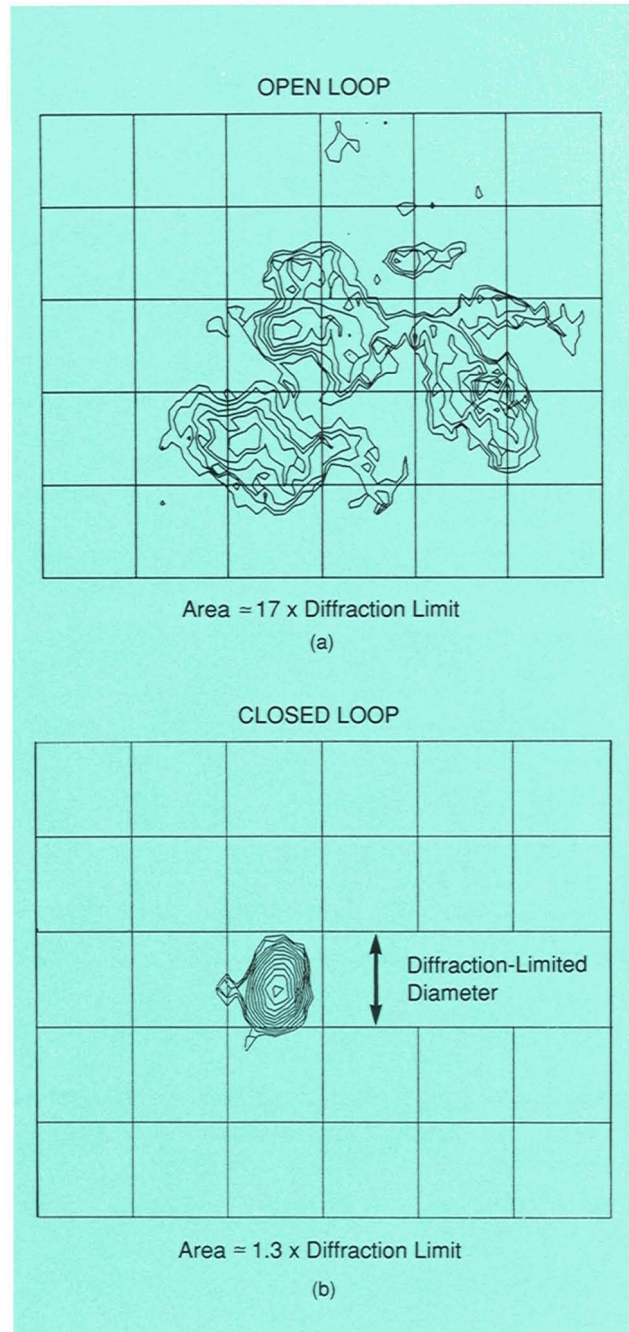


Fig. 14 — The performance of the adaptive-optics system as indicated by beacon far-field-intensity profiles. The contour interval is 2 dB, and the outermost contour encloses 63% of the received flux. (a) Performance without adaptive compensation. (b) Performance with adaptive compensation.

nearly the diffraction limit.

An initial series of tests without Raman amplification were performed to characterize the ability of the adaptive-optics system to compensate

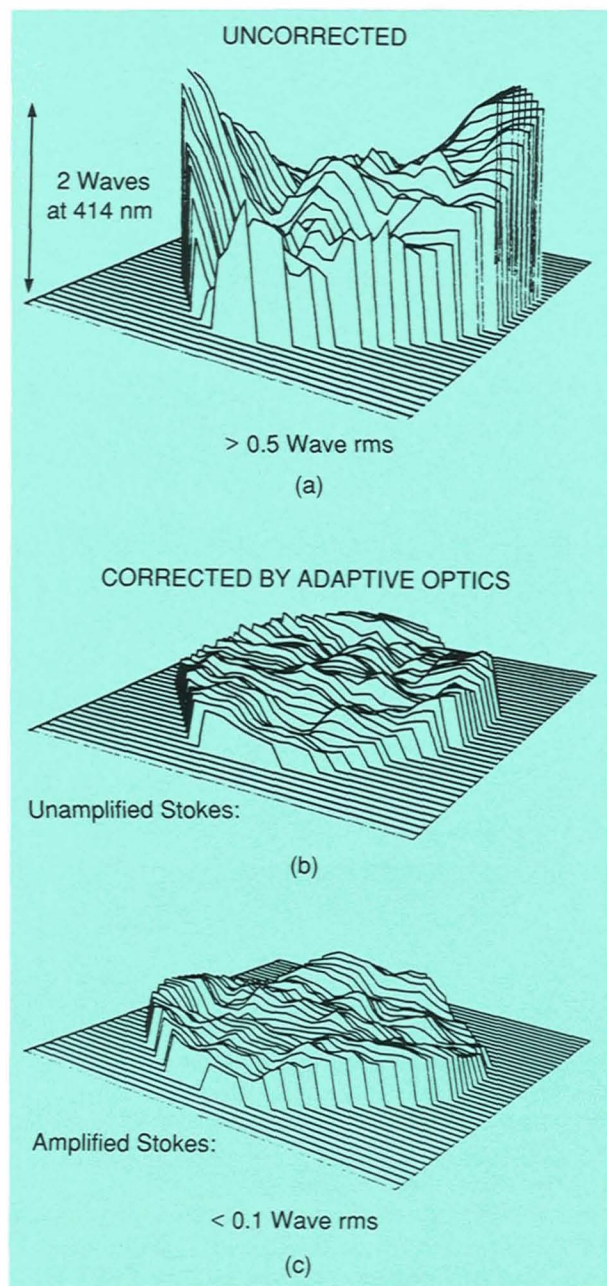


Fig. 15— Stokes beam quality after passing through phase screens. (a) Stokes phasefront without adaptive compensation. (b) Stokes phasefront with adaptive compensation applied but without amplification. This profile indicates the baseline performance of the adaptive-optics system independent of the Raman amplifier. (c) Stokes phasefront with adaptive compensation applied and with amplification. No further reduction in beam quality is observed when the Raman amplifier is active.

the Stokes beam. The pump beam was blocked at the entrance to the pump/Stokes dichroic, and the Stokes beam passed through the Raman

amplifier without experiencing gain. The beam attenuator at the amplifier exit was removed to increase the amount of Stokes light entering the diagnostics, and a series of tests were made both with and without the adaptive-optics loops active.

Once the adaptive-optics-system baseline performance was determined, the Stokes-beam attenuators were replaced and the pump beam was allowed to enter the Raman amplifier. As before, the adaptive-optics phase loops are active while the excimer laser is charged and fired. The Stokes beam, after receiving the adaptive-optics correction, is amplified to a level of approximately 75 J (which corresponds to 50% conversion). At the amplifier exit a 100-mJ sample is removed from the beam and directed out through the phase screens into the diagnostics.

Figure 15 shows the results of this sequence, with reconstructed Stokes phasefronts produced from shearing-interferogram data. Figure 15(a) shows the Stokes phasefront that results from passage through the phase screens without adaptive compensation. The phase screens cause severe aberration, with an rms phase distortion of 0.55 wave (at 414 nm) and a peak-to-peak deviation of nearly two waves. Figure 15(b) shows the phasefront produced when the adaptive-optics correction is applied by the deformable mirror, but the pump beam is blocked, so no amplification occurs. The Stokes wavefront error is significantly reduced. The peak-to-peak excursion is approximately 0.3 wave with 0.1-wave rms residual phase error. This error represents the baseline performance of the adaptive-optics system.

Figure 15(c) shows the Stokes phasefront measured when both the adaptive-optics correction is active and the amplifier is operating at high gain. The Stokes wavefront error is reduced significantly with a peak-to-peak wavefront error of approximately 0.3 wave and 0.1 wave rms. The important result here is that the phasefronts in Fig. 15(b) and (c) are *quantitatively similar* — the amplification process has not significantly modified the Stokes phasefront.

Figure 16 shows amplified Stokes beam far-

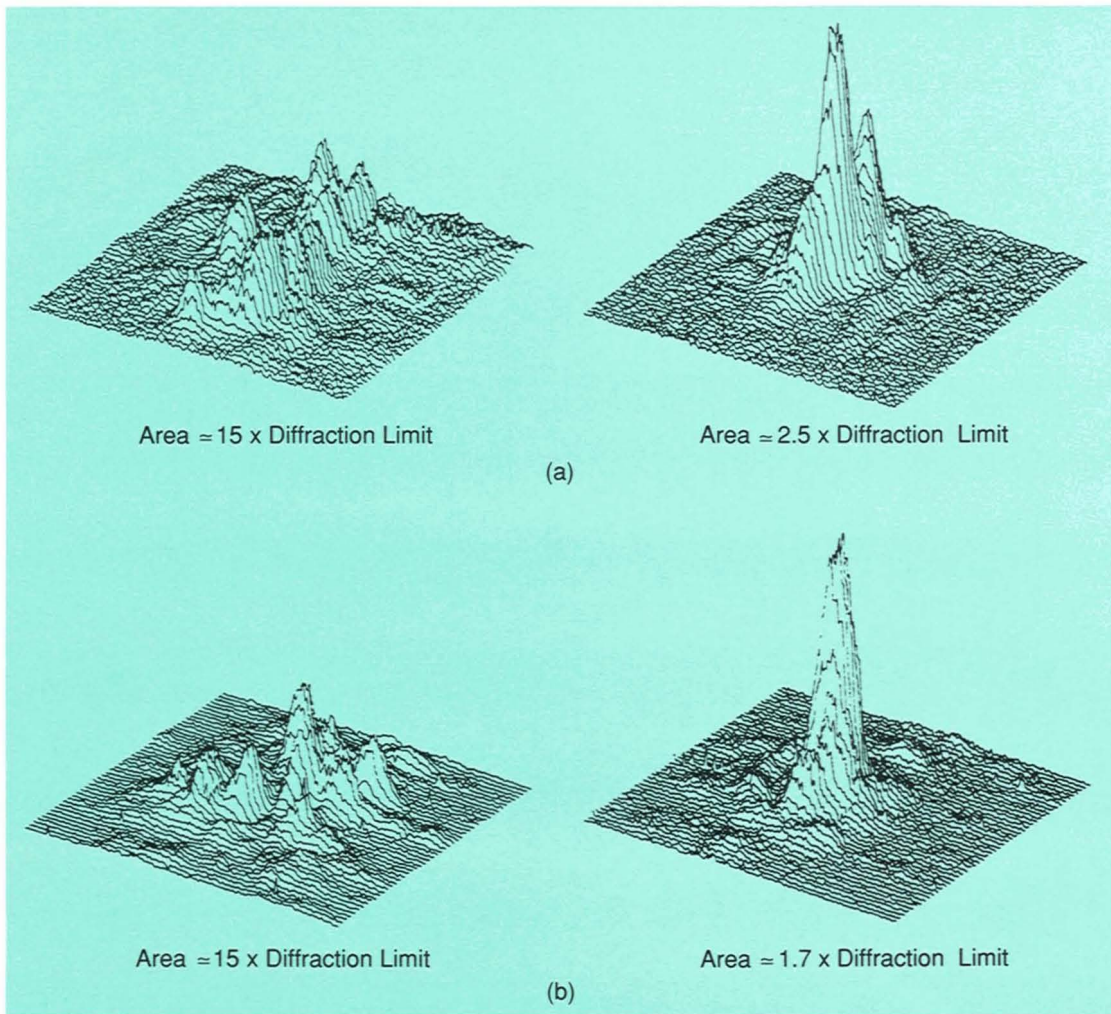


Fig. 16— Amplified Stokes far-field irradiance profiles for two different turbulence realizations. For both (a) and (b) the data on the left show results without adaptive compensation; the data on the right side show results with adaptive compensation. With adaptive compensation, the amplified Stokes far-field irradiance approaches the diffraction limit.

field irradiance profiles recorded during sequences similar to the one just described. For each test sequence a different turbulence realization was used, i.e., a different phase screen. In both Fig. 16(a) and Fig. 16(b) the isometric projection on the left side shows the Stokes far-field irradiance without adaptive correction. As in the beacon data recorded at the entrance to the wavefront sensor, the phase screens impart a significant distortion, which results in a far-field area of approximately 15 times the diffraction limit.

The data reproduced on the right side of Fig. 16(a) and Fig. 16(b) are the Stokes far-field spots recorded when the adaptive-optics loops are

active. The precorrection imposed by the deformable mirror is removed upon passage through the phase screens, resulting in high-quality focal spots. In Fig. 16(a) the distortion amounts to 2.5 times the diffraction limit; in Fig. 16(b) the distortion amounts to 1.7 times the diffraction limit.

Figure 17 presents the same data in different form. The upper pair and lower pair of data are false-color contours of the focal profiles shown in Fig. 16(a) and Fig. 16(b), respectively.

#### Results of Numerical Model

The results of the look-through experiments were compared to a numerical model developed

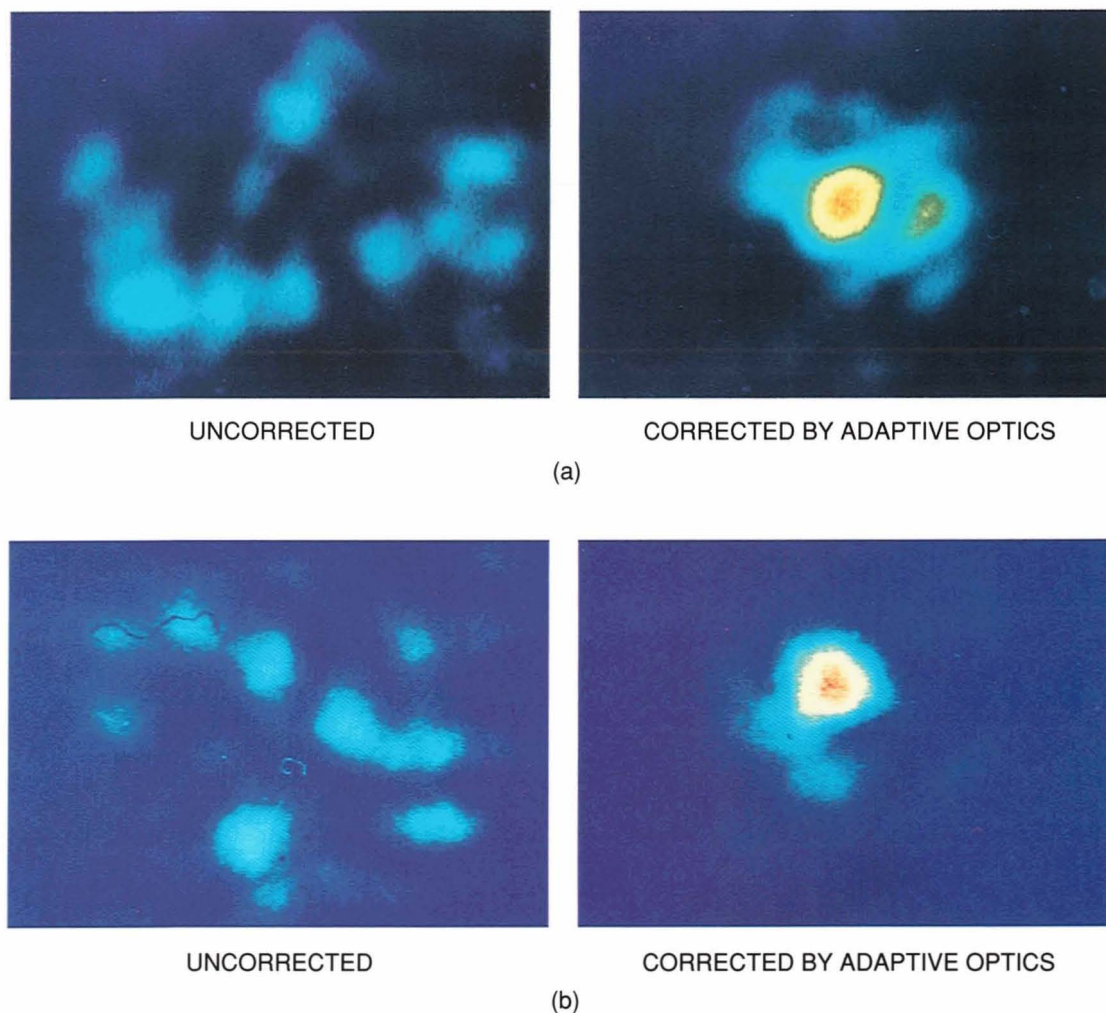


Fig. 17 — Amplified Stokes far-field irradiance presented as false-color contours. The same data are presented as profiles in Fig. 16.

at Lincoln Laboratory. A computer code simulates the laboratory configuration of collimated pump and Stokes beams with an amplifier Fresnel number of 800 and a Stokes injection ratio  $I_s/I_p$  of  $5 \times 10^{-4}$ . The total gain,  $gI_pL$ , is adjusted to achieve the desired energy conversion of approximately 50% from pump beam to Stokes beam. The calculation is a fully three-dimensional, wave-optics treatment including diffraction. Steady-state scattering is assumed (i.e., no time dependence) and the production and growth of an anti-Stokes wave is included.

The initial or input Stokes beam is assigned a phasefront generated by a numerical model of atmospheric turbulence. The magnitude of the

phasefront aberration in the calculation is chosen to resemble quantitatively the aberration produced by the phase screens used in the experiment. Figure 18(a) shows this input Stokes phasefront. The peak-to-valley distortion is 1.7 waves with an rms value of 0.4 wave at 414 nm. The input pump beam is assigned an intensity profile similar to the experimentally measured profile in Fig. 8(b). Figure 18(b) shows a center slice of the intensity profile used in the simulation.

With starting conditions specified, the calculation solves the coupled Raman equations as a function of distance into the amplifier cell. At the cell exit the amplified Stokes beam is com-

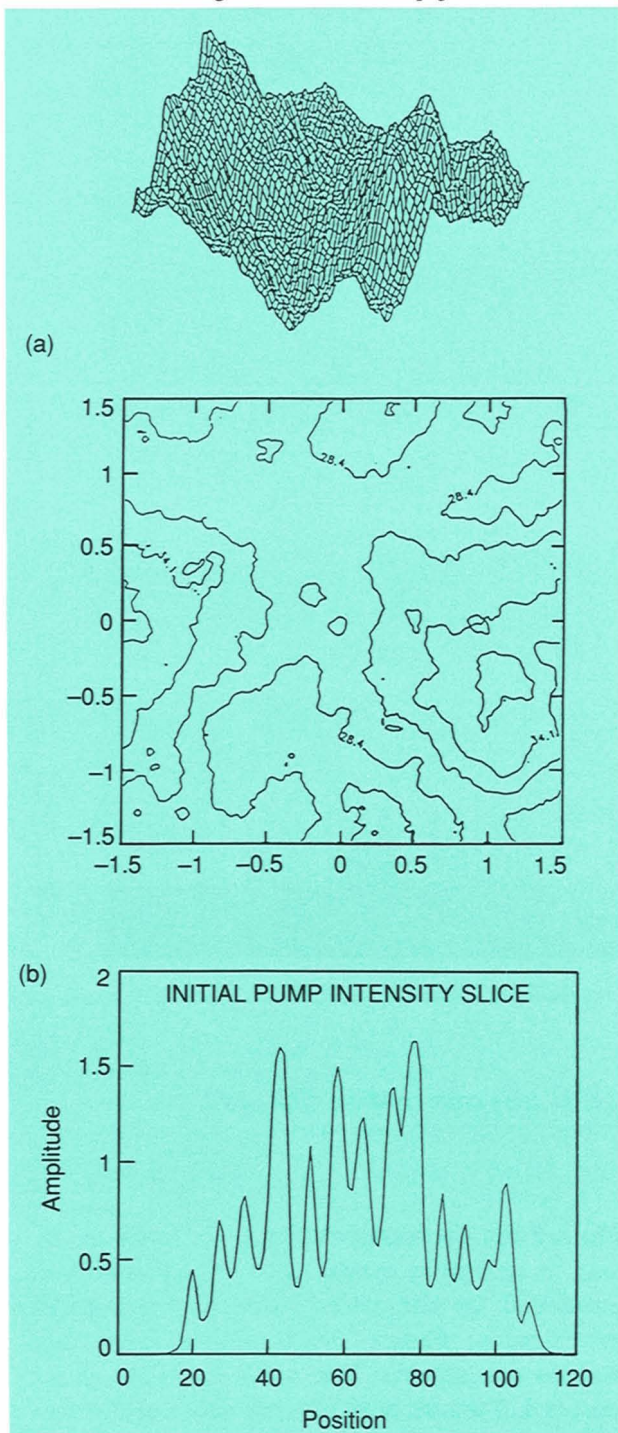


Fig. 18 — Starting conditions for computer simulations for look-through experiments. (a) Phasefront of the input Stokes beam. The contour plot is on the bottom and the surface plot of the same data is on the top. (b) Horizontal slice of initial pump-beam-intensity profile.

pared to the input Stokes beam. To simulate the effect of the precompensated amplified Stokes beam passing through the phase screens, the

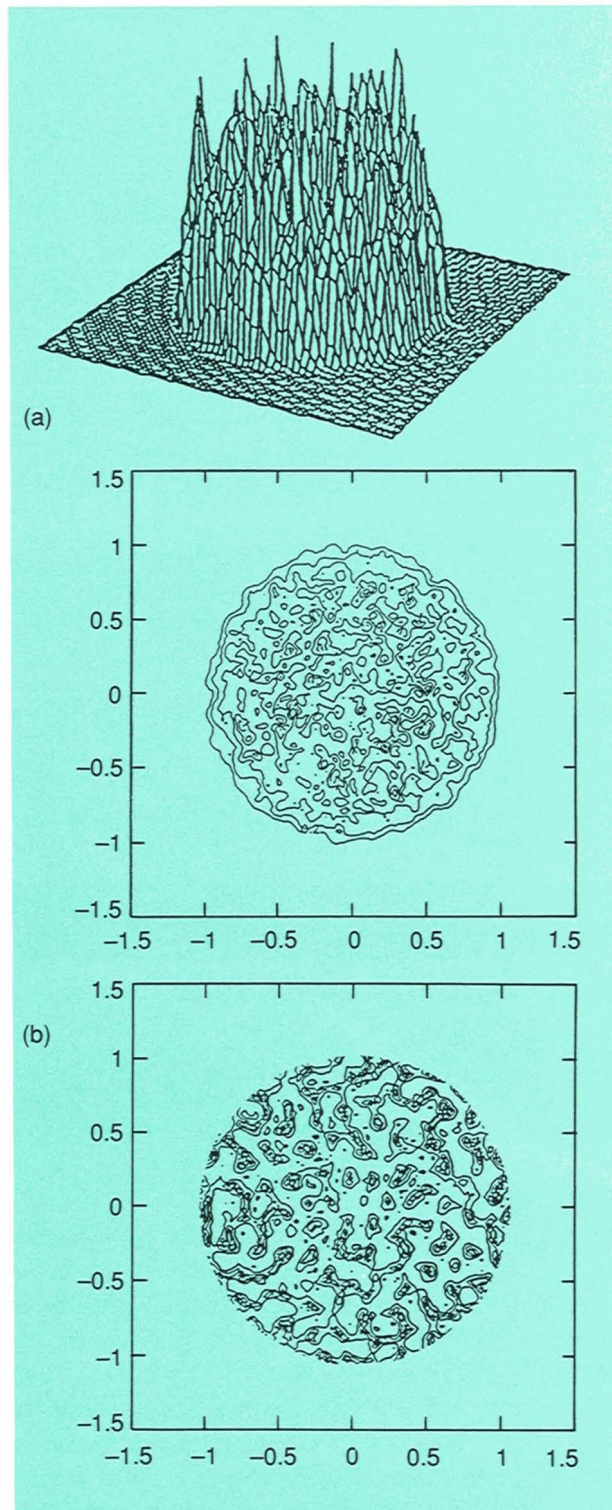


Fig. 19 — Results of computer simulation of look-through experiment. (a) The intensity profile of the amplified Stokes beam. (b) The phasefront difference between the input and output Stokes beams. The residual high spatial-frequency modulation is a direct consequence of the high-frequency modulation on the initial pump-beam-intensity profile in Fig. 18(b).

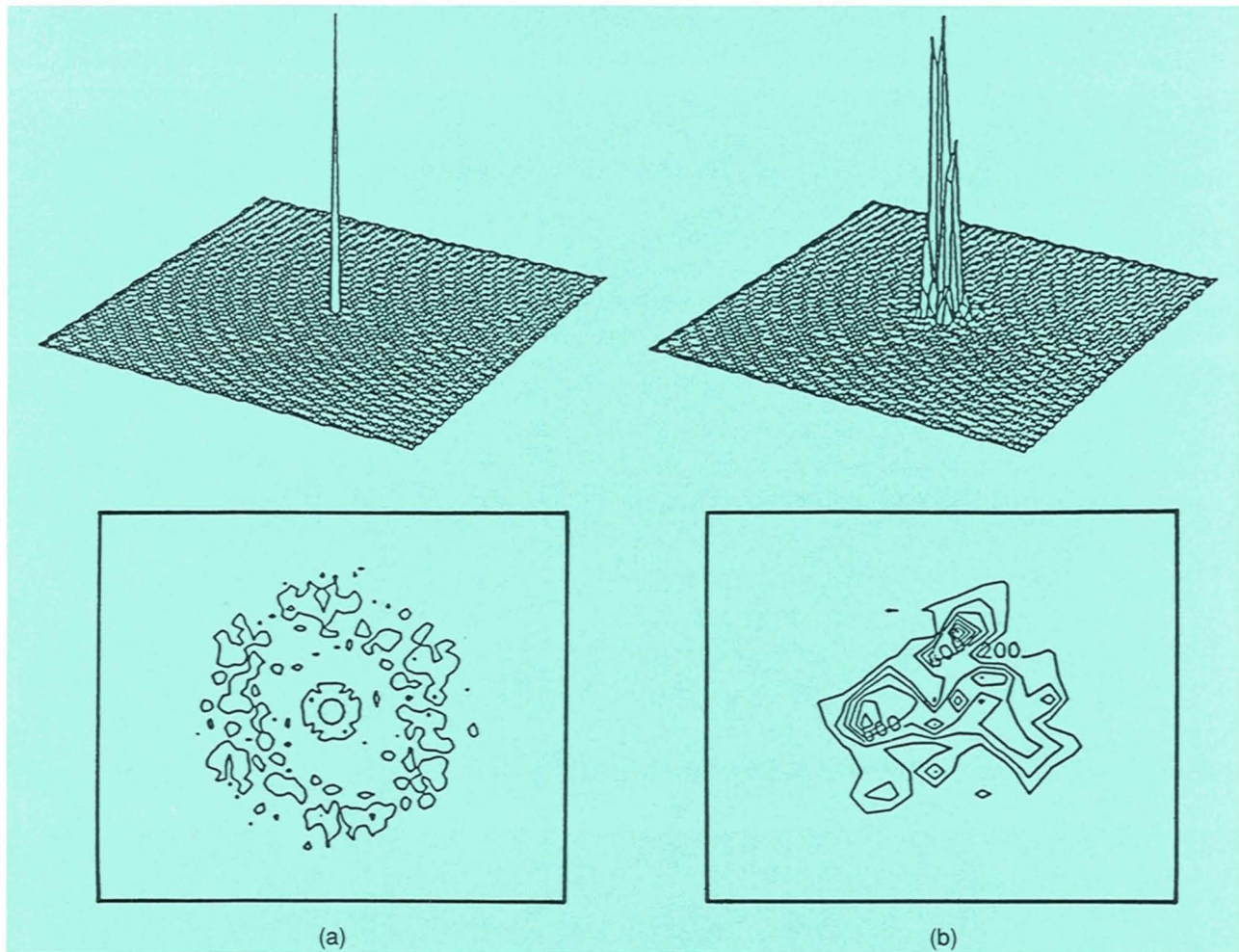


Fig. 20 — Results of computer simulation showing compensated and uncompensated Stokes beams. (a) The amplified Stokes far-field irradiance predicted for compensated turbulence. The low-energy halo outside the central peak is a direct result of the high-spatial-frequency structure shown in Fig. 19(b). (b) The far-field irradiance predicted for no compensation. The vertical peak is approximately one-tenth the amplitude of the compensated peak in (a). It has been enlarged to show peak structure.

input Stokes phasefront (the same phasefront imposed on the beacon by the phase screens) is subtracted from the amplified Stokes phasefront. When appropriate re-imaging is performed, transmission through the phase screens results in the same subtraction. Thus, to simulate the compensated input to the focal-plane diagnostics, a complex field,  $E_{comp}$ , is formed with the calculated amplitude of the amplified Stokes,  $A_{out}$ , and the phasefront difference between amplified and input Stokes

$$E_{comp} = A_{out} e^{i(\phi^{out} - \phi^{in})}. \quad (1)$$

The Fourier transform of this complex field is

then used to predict the far-field irradiance of the Stokes beam that has traversed the phase screens.

Figures 19 and 20 show the results of these calculations. Figure 19(a) shows the intensity profile of the amplified Stokes beam. Note that the intensity modulation on the input pump beam imposes a similar modulation on the Stokes beam. Figure 19(b) shows the phase difference,  $\phi^{out} - \phi^{in}$ , between the amplified and input Stokes phasefronts. The residual phasefront error, induced by the amplification process, approximately 0.09 wave rms at 414 nm, is not removed by the compensation system. For the particular pump-beam profile used

here, this is the penalty for amplification.

Figure 20(a) shows a focal spot derived from the field given in Eq. 1, along with a focal spot calculated directly from the output Stokes beam (Fig. 20 [b]). Notice the high quality of the compensated spot: its area is approximately 1.4 times the diffraction-limited value. Other computer simulations indicate the departure from the diffraction limit is due almost entirely to the intensity modulation of the input pump. Less severe intensity modulation produces less structure on the amplified Stokes phasefront and, as a consequence, less scatter in the focal plane. For example, given the same geometry and gain as above, a depth of modulation equal to approximately one-third of that shown in Fig. 18(b) results in a residual phasefront error of only 0.02 wave rms at 414 nm.

## Summary

The ACE adaptive-optics system was used with a high-gain, large-Fresnel-number Raman amplifier. Successful compensation of simulated atmospheric turbulence demonstrated the feasibility of the Raman look-through technique. The effect of pump-intensity modulation on the amplified Stokes phasefront was determined experimentally, and the results are in good agreement with computer simulations. By choosing appropriate amplifier geometry, the effects of pump-beam-intensity modulation can be minimized, and a high degree of phasefront preservation can be achieved. The results of these experiments will help identify potential problems in applying the Raman look-through technique to field-scale, ground-based lasers.

Follow-on laboratory experiments could replace the adaptive-optics system (wavefront sensor and deformable mirror) with a nonlinear phase conjugator (utilizing stimulated Brillouin scattering, for example [4]). The follow-on experiments could also investigate alternative pumping geometries, such as off-axis pumping

by several overlapping beams (known as Raman beam combining) [13]. Other Raman transitions could also be considered.

## Acknowledgments

The authors wish to acknowledge the Avco Research Laboratory team headed by Daniel W. Trainor. Their expertise in the control and diagnostics of high-power excimer lasers was critical to the success of this effort. We also wish to thank Frank C. Herne for his able assistance during the initial setup, M. Harry Sagerian and Martin J. Brennen for their help in data reduction, and Paul A. Reiser for programming support during the computer simulations.

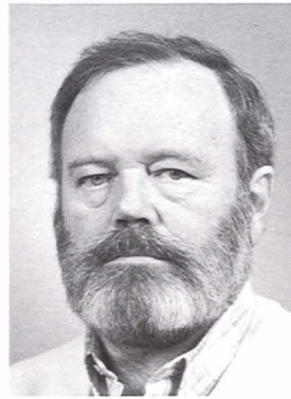
## References

1. J.W. Hardy, "Real-Time Atmospheric Compensation," *J. Opt. Soc. Am.*, **67**, 361 (1977).
2. J.E. Pearson, "Atmospheric Turbulence Compensation Using Coherent Optical Adaptive Techniques," *Appl. Opt.* **15**, 662 (1976).
3. I.C. Winkler, M.A. Norton, and C. Higgs, "Adaptive Phase Compensation in a Raman Look-Through Configuration," *Opt. Lett.* **14**, 69 (1989).
4. Y.R. Shen and N. Bloembergen, "Theory of Stimulated Brillouin and Raman Scattering," *Phys. Rev. A* **137**, 1787 (1965).
5. J. Goldhar and J. Murray, "An Efficient Double-Pass Raman Amplifier with Pump Intensity Averaging in a Light Guide," *IEEE J. Quant. Elect.* **QE-20**, 772 (1984).
6. S.F. Fulghum, D.W. Trainor, C. Duzy, and H.A. Hyman, "Stimulated Raman Scattering of XeF Laser Radiation in H<sub>2</sub> — Part II," *IEEE J. Quantum Electron.* **QE-20**, 218 (1984).
7. R.F.S. Chang, R.H. Lehmberg, M.T. Duignan, and N. Djeu, "Raman Beam Cleanup of a Severely Aberrated Pump Laser," *IEEE J. Quantum Electron.* **QE-21**, 477 (1985).
8. V.V. Bocharov, A.Z. Grasyuk, I.G. Zubarev, and V. Mukilov, "Influence of Spectral Linewidth of Exciting Radiation on the Gain in Stimulated Raman Scattering," *Sov. Phys. JETP* **29**, 235 (1969).
9. E.A. Stappaerts, W.H. Long, and H. Komine, "Gain Enhancement in Raman Amplifiers with Broadband Pumping," *Opt. Lett.* **5**, 4 (1980).
10. A.M. Flusberg and D. Korff, "Transient Refractive-Index Changes in Stimulated Raman Scattering," *J. Opt. Soc. Amer.* **B3**, 1338 (1986).
11. W.H. Long, "Focal Conversion," private communication.
12. C. Duzy, D. Korff, A. Flusberg, and J. Daugherty, "Stokes Wavefront Preservation in Broad-Band Forward Raman Amplification," *IEEE J. Quantum Elect.* **QE-23**, 569 (1987).
13. S.J. Pfeifer, "Multiline Raman Beam Combination," *J. Opt. Soc. Am.* **B3**, 1368 (1986).



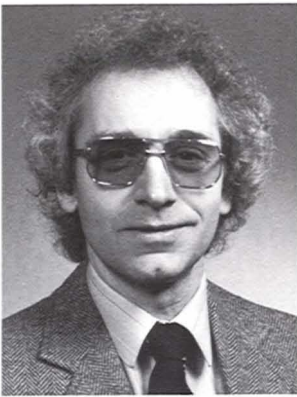
CHARLES HIGGS is a staff member in the High Energy Laser Systems Technology Group. His research interest is in the area of adaptive and nonlinear optics. He received a B.S. degree in physics from Miami University (Ohio), and a Ph.D. in physics from Rice University. In 1988 Chuck shared the Best Paper Award at the Conference on Lasers and Electro-Optics in Boulder, Colorado.

received a B.S. degree in physics from Miami University (Ohio), and a Ph.D. in physics from Rice University. In 1988 Chuck shared the Best Paper Award at the Conference on Lasers and Electro-Optics in Boulder, Colorado.



EMORY D. ARIEL is an assistant staff member in the High Energy Laser Beam Control and Propagation Group. He has been at Lincoln Laboratory for 30 years. He received his bachelor's degree in mechanical engineering from Northeastern University.

years. He received his bachelor's degree in mechanical engineering from Northeastern University.



BRIAN E. PLAYER is in the High Energy Laser Beam Control and Propagation Group, as a subcontractor from Ford Aerospace Corporation. His research focus is in optical sensors. He was previously employed by the Avco Research Laboratory, and he has been at Lincoln Laboratory for 14 years. Brian's B.A. in physics is from Northeastern University.

in optical sensors. He was previously employed by the Avco Research Laboratory, and he has been at Lincoln Laboratory for 14 years. Brian's B.A. in physics is from Northeastern University.



LEE C. BRADLEY, III is a senior staff member in the High Energy Laser Beam Control and Propagation Group. His research interest is in nonlinear optics, and he has been at Lincoln Laboratory for 24 years. Lee received a B.A. in physics from Princeton University and a Ph.D. degree in physics as a Rhodes Scholar at Oxford University.

and he has been at Lincoln Laboratory for 24 years. Lee received a B.A. in physics from Princeton University and a Ph.D. degree in physics as a Rhodes Scholar at Oxford University.